On the Differing Sensitivity to Chemical Gating of Single and Double Layer Epitaxial Graphene Explored Using Scanning Kelvin Probe Microscopy

Ruth Pearce,[†,*] Jens Eriksson,[‡] Tihomir Iakimov,[‡] Lars Hultman,[‡] Anita Lloyd Spetz,[‡] and Rositza Yakimova[‡]

[†]National Physical Laboratory, Teddington TW11 0LW, United Kingdom, and [‡]Department of Physics, Chemistry and Biology, Linköping University, SE-58183 Linköping, Sweden

ABSTRACT Using environmental scanning Kelvin probe microscopy, we show that the position of the Fermi level of single layer graphene is more sensitive to chemical gating than that of double layer graphene. We calculate that the difference in sensitivity to chemical gating is not entirely due to the difference in band structure of 1 and 2 layer graphene. The findings are important for gas sensing where the sensitivity of the electronic properties to gas adsorption is monitored and suggest that single layer graphene could make a more sensitive gas sensor than double layer graphene. We propose that the difference in surface potential between adsorbate-free single and double layer graphene, measured using scanning kelvin probe microscopy, can be used as a noninvasive method of estimating substrate-induced doping in epitaxial graphene.

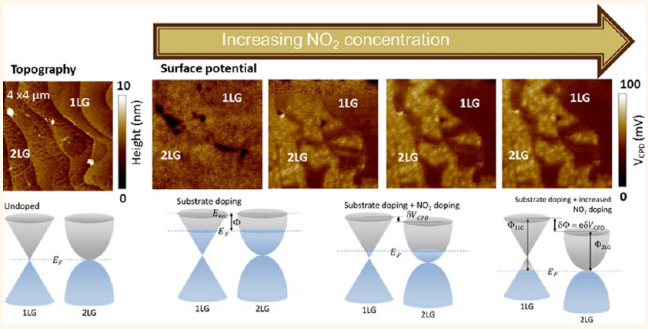

KEYWORDS: epitaxial graphene · environmental gating · scanning Kelvin probe microscopy (SKPM) · gas sensor · thickness dependence

The unique band structure of graphene with its linear and vanishing density of states about the Dirac point makes it extremely sensitive to chemical gating,[1] whereby the Fermi level (E_F) demonstrates large changes with small changes in carrier concentration (n), which can be caused by adsorbed molecules donating or withdrawing electrons. Graphene also demonstrates high chemical stability, low electronic noise[2] and has every atom at the surface, making it an attractive material for gas sensing. Indeed, the sensitivity of graphene to the sorption of gas molecules is such that it may be possible to observe a measurable change in electronic properties upon desorption of a single NO_2 molecule.[3]

Epitaxially growing graphene on SiC is arguably the most attractive method of producing graphene for electrical components due to the large areas of continuous graphene produced along with a high degree of layer thickness homogeneity.[4] Control over the number of graphene layers is important for device manufacture as layer thickness affects the electronic properties of graphene. Recent research[5] has led to an increased understanding of the processes involved in both layer thickness homogeneity and the n-type doping of graphene produced in this way, indicating that control over the SiC substrate morphology could lead to control of the number of graphene layers and charge carriers in as-grown epitaxial graphene (EG). Control over the thickness of the graphene layers has been shown to affect the gas sensitivity of EG,[6] with one layer graphene (1LG) exhibiting extreme sensitivity to NO_2 whereas multilayer epitaxial graphene (MLG) showed a significantly reduced response.

* Address correspondence to ruth.pearce@npl.co.uk.

Received for review November 12, 2012 and accepted April 30, 2013.

Published online April 30, 2013
10.1021/nn3052633

The thickness of EG on SiC cannot be determined by light interference microscopy as has been demonstrated on SiO_2 substrates[1] and requires measurement by other means. Due to the complex morphology of the SiC substrate and layers of adsorbed gases, determination of local thickness variations in epitaxial graphene by standard atomic force microscopy (AFM) is often infeasible. However, AFM coupled with electrostatic force measurements between the tip and the graphene sample (surface potential mapping) can be used to study nanoscale variations in the graphene thickness homogeneity.[7] Surface potential maps from many EG samples were collected and have been compared to low energy electron spectroscopy (LEEM) to validate the accuracy of the SKPM layer coverage estimate.[5] The resulting Scanning Kelvin Probe Microscopy (SKPM) image is a map of the contact potential difference (V_{CPD}) between tip and sample which, in turn, shows the variations in the work function of graphene (Φ). The change in V_{CPD} could be visualized as changes in the Fermi energy (E_F)[8] caused by gating if the layers were not in electrical contact. Maps of these variations in V_{CPD} depict layer thickness in epitaxial graphene (EG). With differences in V_{CPD} for differing thickness of EG theorized to be due to interlayer screening,[9,10] a shift of the C 1s core level toward lower binding energies as the number of layers increases[11] or differences in the energy dispersion and doping between 1 and 2LG.[12] Reports of the difference in V_{CPD} or surface potential values between 1 and 2LG vary with values of $\approx$25 mV being reported for EG under ambient conditions,[7] 100−130 mV in vacuum[9,11,13] and 66 mV for exfoliated graphene on SiO_2 under ambient conditions.[12] This variation in reported surface potential (V_{CPD}) values between 1LG and 2LG, henceforth referred to as 1LG−2LG δV_{CPD}, has been theorized to be due to different substrate induced doping levels in the graphene samples which, due to the different energy dispersions of 1 and 2LG, cause differences in the measured V_{CPD} difference between 1 and 2LG.[12]

The effect of the SiC substrate on the band structure and carrier concentration, *n*, of single and few layer EG has been investigated using angle resolved photoelectron spectroscopy (ARPES), *e.g.*,[14,15] and theoretically[16,17] with 1LG on the Si face of SiC demonstrating a linear energy dispersion about the Dirac point and 2LG thought to have a parabolic energy dispersion.[18] For EG under vacuum conditions (no atmospheric gating), the E_F is positioned above the Dirac point due to substrate interactions[16,17] with interlayer screening reducing this effect with increasing layer number.[10,19] In ambient conditions, with electron withdrawing oxygen and water vapor on the surface, the E_F of EG is generally observed to be close to the Dirac point.[15] The SiC substrate induced *n* has been treated theoretically[16] for 1 and 2LG with two regimes observed; for high *n* ($n \geq \sim 3 \times 10^{13}$ for 1LG equivalent to 0.4 eV), Fermi level pinning is calculated to occur; however, if the SiC induced *n* is lower, E_F is not thought to be pinned and is therefore sensitive to gating. The responsivity, change in *n* with gating, is theorized be different for 1 and 2LG.[16]

Reports of *n* in EG vary depending on the growth conditions and substrate preparation;[20] however, Hall measurements carried out on EG produced using the same method, equipment, and substrates, as reported here, show comparatively very low values of *n*, usually in the range of $(1-2) \times 10^{12}$ cm^{-2}.[21]

There is some debate as to whether 2L EG exhibits a band gap due to SiC substrate interaction.[22,23] Electronic band gap opening in 2LG has been shown for graphene on SiO_2 with a dual gate device[24] and band gap opening in EG due to chemical gating[25,14,26] has been demonstrated. If large enough band gaps can be opened at room temperature, 2LG could be envisaged to make extremely sensitive chemical actuators.

Here we investigate the differing sensitivity of 1LG and 2LG to chemical gating by exposing graphene samples to electron donating and withdrawing gases and monitoring the change in Φ using SKPM. The work function of a material can be changed by an adsorbed molecule through withdrawing (donating) electrons which lowers (raises) E_F (band bending in a semiconductor), or, if the adsorbant forms a strong dipole (such as adsorbed water vapor) by changing the electron affinity of the material. As the experiments presented are carried out in dry conditions, it is assumed that the changes in Φ observed are due to changes in E_F and not due to changes in the electron affinity of graphene. We show that the difference in Φ between 1LG and 2LG not only depends on the substrate induced doping levels of the graphene, but also changes with gating caused by adsorbed gas molecules. We demonstrate that 1LG is more sensitive to chemical gating than 2LG and we calculate that the different band structures of 1 and 2 layer graphene account for a large part, but not all, of the increased sensitivity of 1LG to chemical gating. Our results also point toward a SKPM based, noninvasive means of not only measuring local layer thickness, but also estimating substrate induced *n* in epitaxial graphene. We propose that as long as the graphene surface is free from adsorbates the local substrate induced *n* can be estimated from the contrast difference in SKPM surface potential maps between 1 and 2 layer graphene which correspond to the difference in E_F between 1 and 2LG.

RESULTS AND DISCUSSION

AFM topography and SKPM potential maps were compared for the same area of graphene under ambient conditions (Figure 1). The SKPM potential maps show different contrast for areas of 2LG and 1LG (Figure 1b), with 1LG showing a lower V_{CPD} than 2LG.

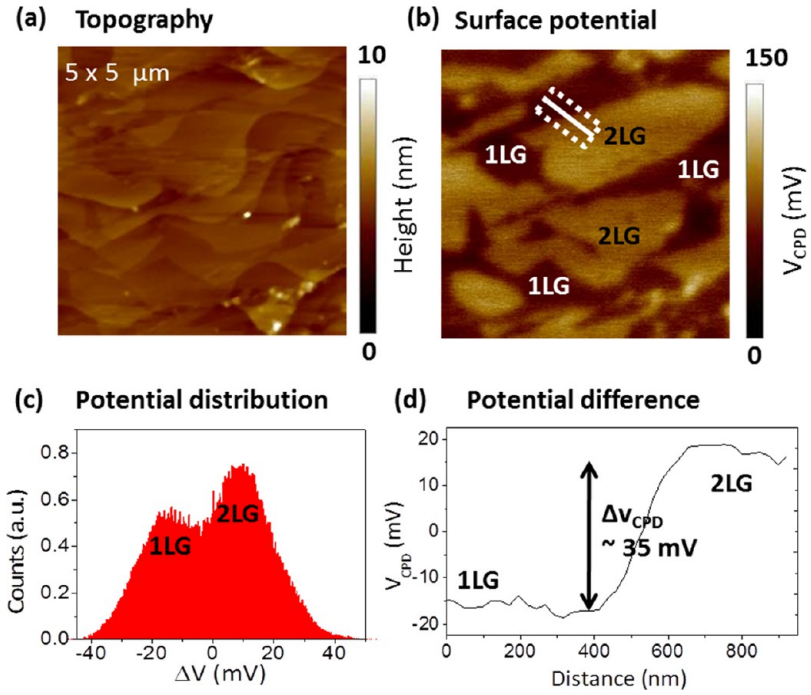

Figure 1. Scanning kelvin probe microscopy (SKPM) images. (a) Topography of an epitaxial graphene (EG) layer; (b) surface potential map showing areas of higher potential corresponding to areas of two layer graphene (2LG); (c) potential distribution histogram averaged over three areas of 5 × 5 μm showing ~60% 2LG; (d) typical 1−2LG δV_{CPD}, taken from the area indicated in (b) showing a value of 35 mV; this 1−2LG δV_{CPD} value was observed over all areas of this sample under normal ambient conditions.

The higher V_{CPD} for 2LG corresponds to a smaller work function for 2LG compared to 1LG. The 1−2LG V_{CPD} difference for this sample under ambient conditions is 35 meV which is similar to reported values for EG under ambient conditions.[7] While measured values for 1−2LG δV_{CPD} were observed to vary between samples, the values are not observed to vary between different areas on the same sample. The value of 35 meV 1−2LG δV_{CPD} was consistent over all investigated areas of this sample while under ambient conditions.

Measurement of the step height between 1LG and 2LG with AFM is difficult for epitaxial graphene samples as areas of 2LG often nucleate at step edges, and during epitaxial growth, graphene layers grow downward into the SiC as Si is sublimed. Figure 2 shows an area of the graphene sample where the graphene has been removed at a scratch. The measured step height between the buffer layer (0LG) and 1LG is ~3.4 Å which is close to reported[27] values (3.34 Å) for interlayer spacing of graphene. The potential map of the same area shows a 1−2LG δV_{CPD} of ~35 meV, indicating that the potential difference shift we observe (~35 meV) corresponds to a difference in thickness of one layer of graphene.

It was observed that while the 1−2LG δV_{CPD} remained constant at ~35 meV under ambient conditions, the absolute V_{CPD} varied significantly (by <100 mV) with different AFM tips and with tip age which is likely to be due to changing tip work function with tip wear and particle pick-up.

To observe if changes in atmospheric conditions affected the 1−2LG δV_{CPD}, scanning was carried out under N_2 at room temperature after surface cleaning to remove adsorbed gases such as oxygen and water vapor. No difference in V_{CPD} was observed between the 1 and 2LG areas under N_2 on any investigated area of the graphene sample (Figure 3a); however, a difference in surface potential of 35 mV was observed almost instantly upon exposing the same sample to ambient conditions again (Figure 3b).

The areas of 2LG were easily identified on the topography scans by the uneven, corrugated appearance of the surface which appeared with repeated vacuum cleaning at 50 °C and ambient exposure. The morphology image of Figure 3b shows an area of corrugated and flat graphene corresponding to areas of 1LG and 2LG with a δV_{CPD} of 35 meV between the flat and corrugated areas observed in the potential maps. The topography image of Figure 3c shows areas of flat 1LG and corrugated 2LG measured in N_2 after the cleaning treatment. While occasional long and separated puckers were observed in areas of 1LG, the corrugated surface effect was only observed for areas of 2LG and was observed on all areas of 2LG making identification of areas of 2LG possible by topographical AFM scanning alone. These surface corrugations are thought to be due to the adsorption of strongly bound gas molecules as carrying out a higher temperature (200 °C) vacuum annealing treatment removed this corrugated effect. Carrying out a cleaning treatment at

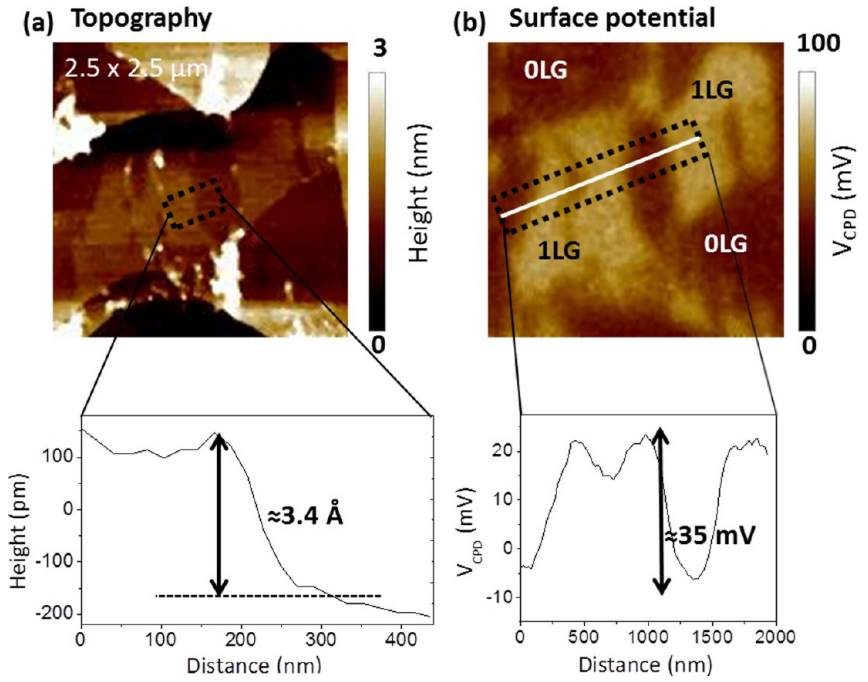

Figure 2. (a) Morphology map showing areas of 1 and 2LG with inset showing a measured buffer layer (0LG)−1LG step height of ∼3 Å taken at the area indicated in the topography image. (b) The corresponding surface potential map with inset showing a potential line profile, taken from approximately the area indicated on the potential scan (centered on the central line and averaged over 30 pixels), demonstrating a ∼35 mV shift for a change in graphene thickness of one layer.

200 °C after a cleaning treatment at 50 °C did not further affect the potential maps (1−2LG δV_{CPD}). The corrugated effect was observed again on areas of 2LG almost immediately after re-exposure to strongly electron donating or withdrawing gases.

Electron withdrawing gases in the lab ambient such as oxygen and water vapor are hypothesized to be responsible for gating the graphene and shifting E_F; however, the strong dipoles of adsorbed water vapor may also affect the measured V_{CPD} by altering the electron affinity of graphene. To investigate if atmospheric gating was responsible for the changing 1−2LG δV_{CPD}, the sample was exposed to NO_2 (1.5 ppm in N_2) which has been shown to act as a p-type dopant to graphene and electron donating gas NH_3 (2 ppm in N_2) which has been shown to be an n-type dopant to graphene.[3] A small amount of each of the aforementioned gas mixtures was flowed into the chamber after vacuum cleaning treatment and purging with N_2 (which does not electronically dope graphene). The gas flow was then stopped and surface topography and potential were mapped (Figure 4).

Figure 4a shows morphology and potential maps of the graphene sample upon initial exposure to 1.5 ppm NO_2 (as soon as the gas flow was switched off). The δV_{CPD} measured between 1LG and 2LG is ∼50 meV; if left for longer in the NO_2 gas mixture, the 1−2LG δV_{CPD} was observed to increase further, upward of ∼100 mV. The increased contrast between 1 and 2LG suggests that the E_F of 1LG has reduced further than the E_F of 2LG due to the adsorption of electron withdrawing NO_2.

Figure 4b shows a morphology and potential map of the graphene sample upon initial exposure to 2 ppm NH_3 in N_2. The areas of 1LG and 2LG are clearly distinguishable in the morphology map by the puckered surface of the 2LG areas and the flat 1LG. After NH_3 exposure, the 1LG areas show a higher V_{CPD} than the 2LG areas which is opposite to observations under electron withdrawing conditions (exposure to NO_2) as seen in Figure 4a. The opposite contrast for 1 and 2LG in the potential map indicates that the E_F of 1LG increased more than that of 2LG due to electron donation from the adsorbed NH_3 molecules.

Figure 4c shows schematic band structures depicting changing Φ with gas environment. In an electron withdrawing environment (with oxygen, water vapor or NO_2 present), 1LG has a larger Φ than 2LG. For stronger electron withdrawing environments, a larger 1−2LG δV_{CPD} is observed. In an electron donating atmosphere (*e.g.*, with NH_3 present), the Φ of 1LG is smaller than that of 2LG. Our experiments show that when gases are desorbed from graphene on SiC 1LG and 2LG have a similar Φ. Chemical gating is understood as a lowering or rising of E_F when gases adsorb on the graphene surface. Due to the narrower density of states around the Dirac point of 1LG, the same change in n brings about a larger change in E_F for 1LG than 2LG.

After NH_3 exposure, the 1−2LG δV_{CPD} values did not return to their original values after the vacuum cleaning treatment which utilized heating to 50 °C; this indicates that the NH_3 was not completely desorbed.

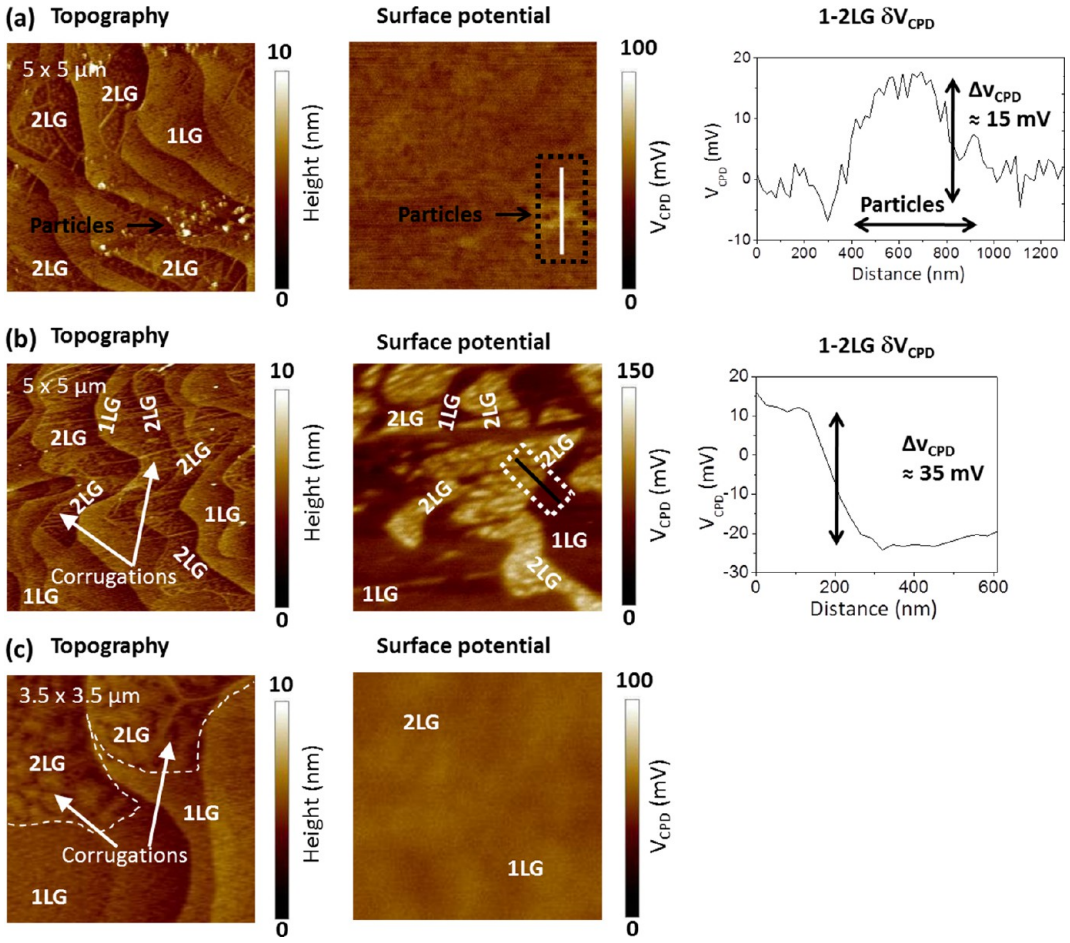

Figure 3. (a) Topography map (left), surface potential map (center), and plot of potential distribution (right), all showing the same area of graphene imaged in N_2 after the cleaning treatment. A change in V_{CPD} is only observed in an area with surface contamination; no contrast change is seen between areas of 1 and 2LG. (b) Topography map (left), surface potential map (center), and plot of potential distribution (right), all showing the same area of graphene imaged under ambient conditions with an observed 1−2LG δV_{CPD} of ∼35 mV. Puckers and surface corrugations are clearly visible on all areas of 2LG. (c) Graphene imaged in N_2 after cleaning treatment: (left) topography map showing surface corrugations for areas of 2LG, (center) surface potential map showing no contrast in V_{CPD}.

Complete desorption was achieved on heating the sample to 200 °C under vacuum ($\times 10^{-6}$ Torr) conditions which also removed the observed corrugated effect on the areas of 2LG. The removal of the corrugated effect observed on the 2LG after high temperature and vacuum anneals suggests that this effect it is due to gas adsorption which changes the topography but not the surface potential of the 2LG.

To illustrate the change in 1−2LG δV_{CPD} on the same area of the graphene sample under different environmental conditions, very dilute electron withdrawing (1 ppm NO_2 in N_2) or donating gas (1.5 ppm NH_3 in N_2) was very slowly leaked into the chamber after the cleaning treatment. High flow rates caused noise in the resonance of the AFM tip, rendering measurements impossible.

Figure 5 illustrates the typical trend in changing surface potential with NO_2 exposure. The same trend was repeatedly observed in other areas of the sample and on other EG samples. Figure 5a,b shows the surface potential and morphology maps of one area of the graphene sample in an N_2 atmosphere with a sufficiently small flow rate of N_2 into the chamber to not disturb imaging. The gas leaking into the chamber was switched to 1.5 ppm NO_2 in N_2 at the same low flow rate at the beginning of scanning of Figure 5c; the scan direction is indicated by the black arrow at the side of each image. Scanning then continued in the NO_2 gas mixture; see Figure 5d. The gas flow was then switched to pure N_2 again at the same very low flow rate, see Figure 5e (the change from NO_2 to N_2 is indicated by the dashed white line). Scanning continued in N_2 in Figure 5f. In a nongating N_2 environment, almost no difference in 1−2LG V_{CPD} is measured; however, as soon as NO_2 is introduced into the chamber an increasing difference in 1−2LG V_{CPD} is observed, indicated by increasing contrast on the surface potential maps. On switching the gas leaking into the chamber to N_2 again the NO_2 gas began to slowly desorb from the graphene surface and the difference between the

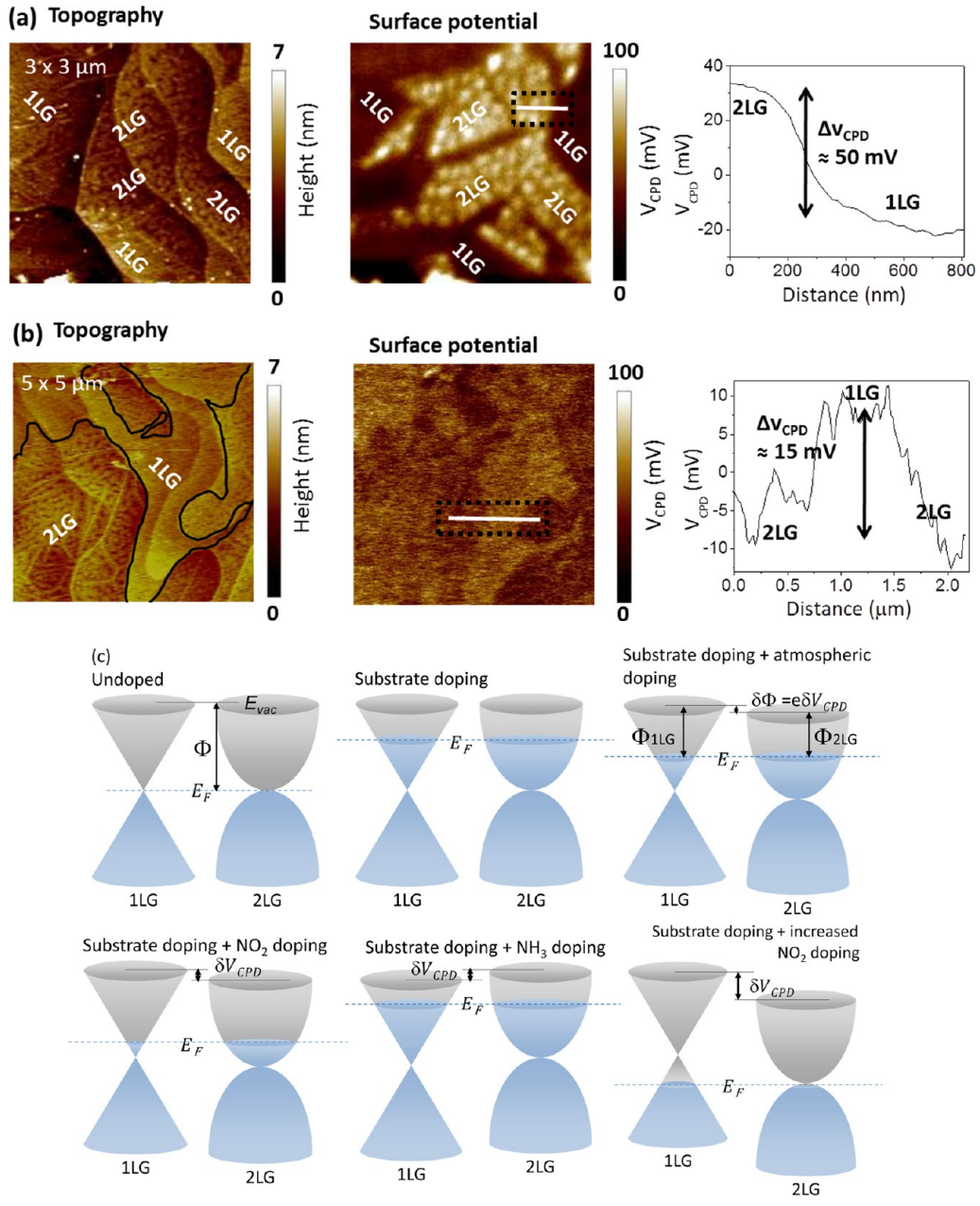

Figure 4. (a) Topographical and potential AFM images showing puckered areas of double layer (2LG) and flatter areas of single layer graphene (1LG) on exposure to 1 ppm NO_2 in N_2; the potential map of the graphene surface shows greater contrast between single layer graphene and double layer graphene than when exposed to ambient conditions. (b) Topographical and potential AFM images showing puckered areas of 2LG and flatter areas of 1LG after exposure to 2 ppm NH_3 in N_2; the potential map of the graphene surface shows a higher surface potential for 1LG than 2LG. (c) Band structure schematics showing changing work function (Φ) with atmospheric gating; in an electron withdrawing atmosphere (*e.g.*, with O_2, H_2O or NO_2 present), 1LG has a larger work function than 2LG. In an electron donating atmosphere (*e.g.*, with NH_3 present), the Φ1LG is smaller than that of 2LG. The difference in Φ between 1 and 2 layer graphene is proportional to the measured δV_{CPD}.

1LG and 2LG surface potential began to gradually decrease. Due to the very low gas flows that could be accommodated during imaging (>1 mL min^{-1}), the concentration of NO in the chamber is expected to be considerably lower than the 1 ppm concentration of the bottle. Each scan took approximately 20 min.

The contrast between the 1LG and 2LG areas in the surface potential maps increases in the presence of NO_2 and decreases again when the NO_2 flow is switched off. The surface potentials of both the 1LG and the 2LG decrease however, the surface potential of 1LG decreases more than that of the 2LG, which appears brighter than the 1LG when NO_2 is present.

Figure 6a shows an unflattened surface potential image when NO_2 is first introduced into the chamber; areas of 1LG and 2LG are marked by the white line. The surface potential decreases during the scan which can be seen in the darkening color of the surface potential

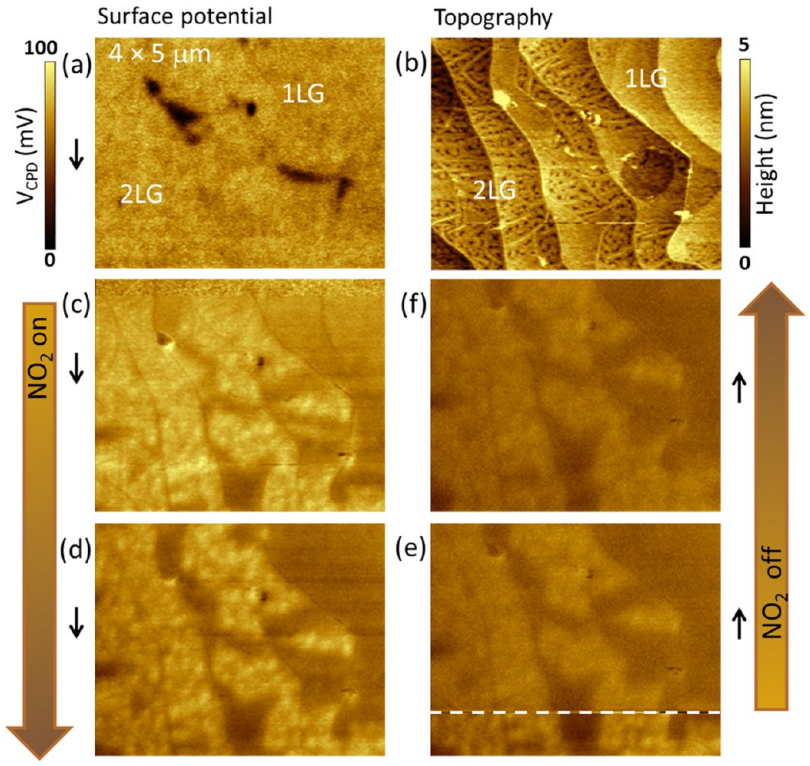

Figure 5. Sequential exposure of graphene to low concentration NO_2 in N_2 showing (a) surface potential map of graphene in N_2, (b) topography map of the same area, (c) surface potential map with N_2 flow changed to NO_2 at the top of the scan, (d) surface potential map with the scan beginning after 40 min in NO_2, (e) surface potential map with NO_2 changed to N_2 at the dashed white line, (f) surface potential map with the scan starting ~45 min after NO_2 was switched to N_2. The scan direction is indicated by the black arrows. The area (4 × 5 μm) is the same on all of the surface potential images.

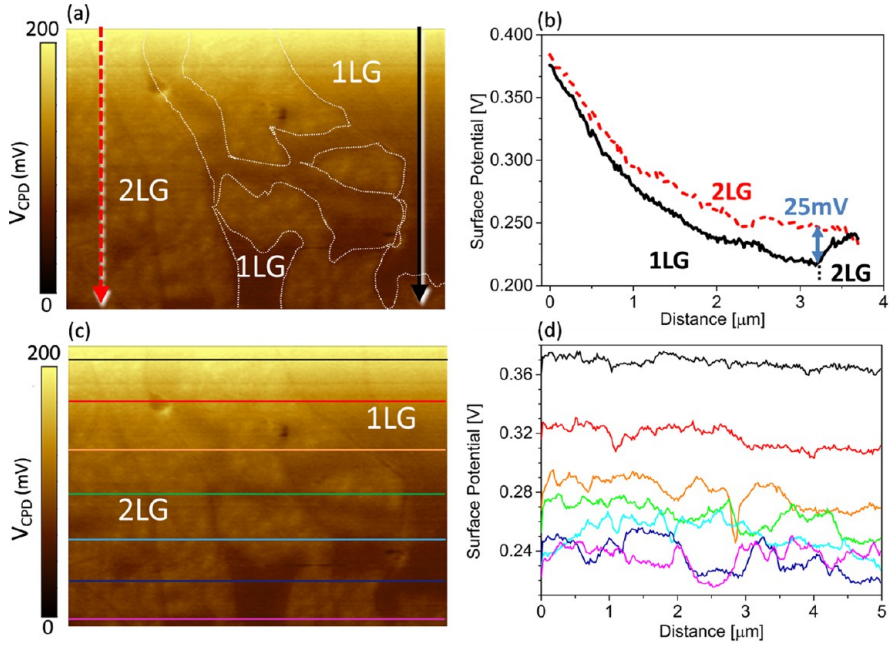

Figure 6. (a) Unflattened surface potential maps showing decreasing surface potential with NO_2 exposure; the white lines show the approximate boundaries between the 1LG and the 2LG, the red and black arrows show the extracted line profiles in panel b; (b) extracted line profiles showing a larger decrease in surface potential for 1 LG than for 2LG; (c) surface potential map showing extracted line profile sites; (d) extracted line profiles showing decreasing surface potential and increasing 1−2LG δV_{CPD} with NO_2 exposure time.

plot. Figure 6b shows the extracted line profiles; the areas of the line profiles are marked in Figure 6a. Under N_2, the difference in surface potential of 1LG and 2LG is small (<5 mV); with increasing NO_2 exposure, the

difference in surface potential of 1LG and 2LG increases to ~25 mV. Figure 6c shows the unflattened surface potential map on initial exposure to NO_2 with colored lines indicating extracted line profiles plotted in Figure 6d. The decrease in surface potential with NO_2 exposure time is initially fast but slows down with increasing NO_2 exposure time as seen in Figure 6d (extracted line profiles are averaged over 10 pixels). V_{CPD} values for 1LG and 2LG were taken from the averaged extracted line profiles as far from the potential steps between 1LG and 2LG as possible in order to reduce any spatial averaging of the values.

Surface potential values for 1LG and 2LG taken from each of the 7 extracted line profiles shown in Figure 6d are plotted in Figure 7 along with the calculated change in n for 1LG and 2LG. The corresponding change in n for 1LG and 2LG was calculated from the extracted surface potential values by assuming the change in absolute V_{CPD} values is proportional to the change in $E_F - \delta E_F \propto e\delta V_{CPD}$ where e is the elemental charge). The change in n was calculated assuming a linear dispersion for 1LG, and a parabolic dispersion for 2LG. A review of the electronic properties of 1LG and 2LG showing equations for elementary electronic quantities in 1 and 2LG is available in ref 28. The 1LG n is proportional to E_F^2; $n = E_F^2/\pi V_F^2\hbar^2$ with $n - \Delta n$ proportional to $(E_F - \delta E_F)^2$ (see eq 1 below). Equation 2 below shows the relationship between the n of 2LG and the measured δV_{CPD}.

$$\Delta n\,1\mathrm{LG} = \frac{2e\delta V_{CPD}\sqrt{n}}{\hbar v_F\sqrt{\pi}} - \frac{(e\delta V_{CPD})^2}{\hbar^2 v_F{}^2\pi} \qquad (1)$$

$$\Delta n\,2\mathrm{LG} = \frac{\delta V_{CPD} e 2m^*}{\hbar^2\pi} \qquad (2)$$

Where n is the carrier concentration in N_2 after cleaning and e is the elemental charge; m^* was taken to be $0.03m_e$ where m_e is the mass of an electron.[28,29] It is assumed here that n 1LG in N_2 is similar to values of $\sim 2 \times 10^{16}\,m^{-2}$ ($2 \times 10^{12}\,cm^{-2}$) from magneto-resistance experiments carried out in vacuum on EG samples produced in the same way.[21] However, it should be noted that the processing involved in creating Hall bar structures for these measurements may affect n from, *e.g.*, photoresist residue, and that there is some small spread in n of epitaxial graphene even when produced under identical conditions.[5] In this model, the change in n for 2LG is not dependent on the initial n. For ease of comparison of Δn, values the initial 2LG n plotted in Figure 7 is that of 1LG ($2 \times 10^{16}\,m^{-2}$); however, if the work function of 1 and 2LG is the same, the initial n for 2LG is expected to be higher than that of 1LG due to the difference in band structure of 1LG and 2LG. It is also assumed that the adsorbed gas does not change the electron affinity of the graphene and the measured changes in V_{CPD} are due to shifts in E_F. For each change

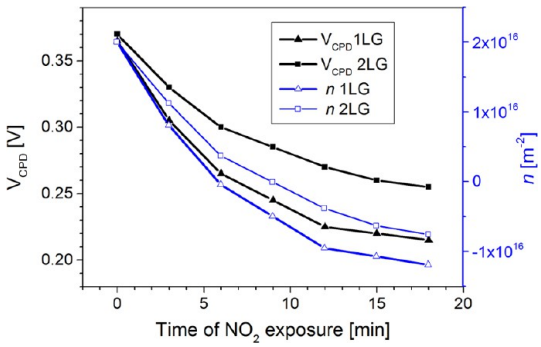

Figure 7. Plot showing change in absolute surface potential of 1LG (closed triangles) and 2LG (closed squares) with increasing NO_2 exposure time (increasing NO_2 concentration). The calculated change in carrier concentration, n, is plotted for 1LG (open triangles) and 2LG (open squares) for increasing time of NO_2 exposure.

in measured V_{CPD}, δn and the resultant n are calculated iteratively for 1LG and 2LG (Figure 7).

It is calculated, see Figure 7, that both 1LG and 2LG undergo an n−p-type transition upon adsorption of less than 1.5 ppm NO_2; this is in agreement with sensing data,[6] where 1L EG was observed to become p-type on adsorption of <300 ppb NO_2. The calculated changes in n for 1LG and 2LG are similar; however, the 1LG n is calculated to decrease more upon NO_2 exposure than the 2LG n. The discrepancy in calculated n could be due to the model used not accurately reflecting the difference in DOS for 1LG and 2LG, or due to inherent errors in the SKPM measurement technique; the extracted δV_{CPD}1−2LG values could be reduced due to spatial averaging, whereby the area under the AFM cantilever contributes to the total V_{CPD} values not just the area under the AFM probe tip.[30,31] This effect could lead to a degree of averaging of values of 1LG and 2LG near to the boundary between 1LG and 2LG; however, this effect would be expected to reduce the difference between measured 1−2LGδV_{CPD}. The changes in n may also have a physical cause. It can be debated that 2LG and 1LG have different speeds of response rather than different sensitivities to chemical gating; however, it is observed (Figure 7) that the plotted values of absolute V_{CPD} begin to stabilize with increasing time as steady state is reached. Differing chemical reactivity rates of 1LG and 2LG have been suggested,[32] and the sticking coefficients of gases on 1 and 2LG may also differ. Increasing hydrophobicity with increasing epitaxial layer thickness has been suggested to be responsible for the observed corrugated surface morphology observed on areas of 2LG.[33] It has also been shown that adsorption of some strongly electron donating and withdrawing molecules onto a graphene surface may induce band gap opening.[25,14] A combination of the different band structure and different gas molecule sticking coefficients and adsorption energies could be hypothesized to be responsible for the different shifts in V_{CPD} for

1 and 2LG demonstrated here with changing gas environments

No V_{CPD} contrast is observed in the potential maps in N_2 environments after cleaning (Figures 5 and 6) which indicates that the work function of 1 and 2 LG are equal under those conditions for this sample. The V_{CPD} contrast for different graphene samples was observed to vary slightly ($\sim\pm5$ mV) for different epitaxial graphene samples. As there is no gating due to gas adsorption under N_2 conditions, this change in V_{CPD} is thought to be due to different levels of substrate induced doping which has been reported for, *e.g.*, different substrate off-cut angles.[5] The substrate induced *n* can be estimated from the 1−2LG δV_{CPD} taken from potential maps if gas exposure history is known or if measurements are carried out in vacuum or an inert gas after annealing. This could lead to a fast and noninvasive method of estimating substrate induced *n* in samples where 1 and 2LG areas can be found. Experiments are ongoing comparing the calculated *n* values from 1 to 2LG δV_{CPD} observed after cleaning with transport measurements on epitaxial graphene samples.

CONCLUSIONS

Using SKPM, we have demonstrated that 1LG shows a larger shift in surface potential upon exposure to electron withdrawing and donating gases than double layer graphene. We have also shown that the contact potential difference measured between 1 and 2 layer graphene (1−2LG δV_{CPD}) depends not only on doping from the substrate, but also on gating from surface adsorbed molecules from the environment. The different sensitivity of 1 and 2LG toward chemical gating is calculated to be largely due to the narrower 1 layer graphene energy dispersion about the Dirac point. This work has implications for gas sensor research and suggests that a well-controlled and homogeneous single layer of graphene is essential in order to optimize sensitivity and arrive at the possibility of single molecule detection. This research also indicates that the 1−2LG δV_{CPD} measured by noninvasive SKPM carried out in vacuum or with cleaned samples in an inert atmosphere can be a useful tool for estimating the substrate induced doping of an EG layer.

METHODS

The EG was prepared by sublimation of SiC and subsequent graphene formation on Si- terminated 4H-SiC substrate at 2000 °C in argon at a pressure of 1 bar.[12] These conditions are conducive to fast surface kinetics due to the high temperature while also favoring a low rate of silicon loss from the surface,[17,12] leading to larger areas of homogeneous graphene than high vacuum and ultrahigh vacuum growth.[13,14] SKPM and LEEM[5] showed these growth conditions produce predominately single layer graphene; however, some samples have areas of 2LG. The sample investigated here had an unusually high surface coverage of 2LG of ~60% as mapped by SKPM.

Surface potential maps were obtained by SKPM performed with a Veeco Enviroscope with Nanoscope IV electronics, which uses an interleave lift mode to record the surface potential. The measurements were performed using conductive, platinum coated Si tips (NT-MDT NSG01/Pt) with resonance frequencies between 98 and 154 kHz. To record the surface potential, the tip follows the stored surface topography at a constant lift height of 10−20 nm above the sample while an ac voltage of 3000 mV was applied to the tip at the resonance frequency of the tip cantilever (ω). The tip DC bias is adjusted to nullify the tip oscillation at ω, which is caused by the contact potential difference (δV_{CPD}) between the tip and the sample surface. The resulting image is a map of the variations in the V_{CPD} between the tip and the graphene, with the variations in the V_{CPD} assumed here to be due to variance in E_F.[15] The work function of the graphene sample (Φ_g) could be quantified if the work function of the tip (Φ_{tip}) was known, $\Phi_g = V_{CPD} - \Phi_{tip}$; however, absolute values of V_{CPD} were found to be difficult to quantify due to changing Φ_{tip} caused by attachment of particles to the tip or removal of tip coating during scanning.

The samples were grounded to the AFM stage using silver paint; as the graphene is continuous, the entire surface of the sample was at ground potential. Measurements were taken either under ambient conditions or with a controlled gas environment. The gas environment inside the sample chamber was controlled by flowing in N_2, 1.5 ppm NO_2 in N_2 or 2 ppm NH_3 in N_2. The flow of each gas was controlled by a regulator and the gas inlet valve on the sample chamber. Graphene surface cleaning treatments were carried out by reducing the pressure in the chamber to between 1×10^{-5} and 1×10^{-6} Torr overnight while heating to 50 °C. Heating to higher temperatures and longer times was tested, but did not affect any further changes in the surface potential maps of the samples, whereas shorter vacuum treatment times or no heating did not lead to reproducible potential maps.

Conflict of Interest: The authors declare no competing financial interest.

Acknowledgment. The authors would like to thank A. Tzalenchuk and T. Burnett for helpful and illuminating discussions.

REFERENCES AND NOTES

1. Novoselov, K. S.; Geim, A. K.; Morozov, S. V.; Jiang, D.; Zhang, Y.; Dubonos, S. V.; Grigorieva, I. V.; Firsov, A. A. Electric Field Effect in Atomically Thin Carbon Films. *Science* **2004**, *306*, 666–669.
2. Liu, G.; Stillman, W.; Rumyantsev, S.; Shao, Q.; Shur, M.; Balandin, A. A. Low-Frequency Electronic Noise in the Double-Gate Single-Layer Graphene Transistors. *Appl. Phys. Lett.* **2009**, *95*, No. 033103.
3. Schedin, F.; Geim, A. K.; Morozov, S. V.; Hill, E. W.; Blake, P.; Katsnelson, M. I.; Novoselov, K. S. Detection of Individual Gas Molecules Adsorbed on Graphene. *Nat. Mater.* **2007**, *6*, 652–655.
4. Yakimova, R.; Virojanadara, C.; Gogova, D.; Syväjärvi, M.; Siche, D.; Larsson, K.; Johansson, L. I. Analysis of the Formation Conditions for Large Area Epitaxial Graphene on Si C Substrates. *Mater. Sci. Forum* **2010**, *645−648*, 565–568.
5. Eriksson, J.; Pearce, R.; Andersson, M.; Iakimov, T.; Virojanadara, C.; Syväjärvi, M.; Gogova, D.; Spetz, A. L.; Yakimova, R. The Influence of Substrate Morphology on Thickness Uniformity and Unintentional Doping of Epitaxial Graphene on Sic. *Appl. Phys. Lett.* **2012**, *100*, No. 241607.
6. Pearce, R.; Iakimov, T.; Andersson, M.; Hultman, L.; Spetz, A. L.; Yakimova, R. Epitaxially Grown Graphene Based Gas Sensors for Ultra Sensitive N O_2 Detection. *Sens. Actuators, B* **2011**, *155*, 451–455.
7. Burnett, T.; Yakimova, R.; Kazakova, O. Mapping of Local Electrical Properties in Epitaxial Graphene Using

Electrostatic Force Microscopy. *Nano Lett.* **2011**, *11*, 2324–2328.
8. Curtin, A. E.; Fuhrer, M. S.; Tedesco, J. L.; Myers-Ward, R. L.; Eddy, C. R.; Gaskill, J. Kelvin Probe Microscopy and Electronic Transport in Graphene on Si C(0001) in the Minimum Conductivity Regime. *Appl. Phys. Lett.* **2011**, *98*, 3595360–3595363.
9. Yu, Y.-J.; Zhao, Y.; Ryu, S.; Brus, L. E.; Kim, K. S.; Kim, P. Tuning the Graphene Work Function by Electric Field Effect. *Nano Lett.* **2009**, *9*, 3430–3434.
10. Guinea, F. Charge Distribution and Screening in Layered Graphene Systems. *Phys. Rev. B* **2007**, *75*, 235433–235440.
11. Hibino, H.; Kageshima, H.; Kotsugi, M.; Maeda, F.; Guo, F. Z.; Watanabe, Y. Dependence of Electronic Properties of Epitaxial Few-Layer Graphene on the Number of Layers Investigated by Photoelectron Emission Microscopy. *Phys. Rev. B* **2009**, *79*, No. 125437.
12. Ziegler, D.; Gava, P.; Güttinger, J.; Molitor, F.; Wirtz, L.; Lazzeri, M.; Saitta, A. M.; Stemmer, A.; Mauri, F.; Stampfer, C. Variations in the Work Function of Doped Single- and Few-Layer Graphene Assessed by Kelvin Probe Force Microscopy and Density Functional Theory. *Phys. Rev. B* **2011**, *83*, 235434–235437.
13. Filleter, T.; Emtsev, K. V.; Seyller, T.; Bennewitz, R. Local Work Function Measurements of Epitaxial Graphene. *Appl. Phys. Lett.* **2008**, *93*, No. 133117.
14. Ohta, T.; Bostwick, A.; Seyller, T.; Horn, K.; Rotenberg, E. Controlling the Electronic Structure of Bilayer Graphene. *Science* **2006**, *313*, 951–954.
15. Riedl, C.; Coletti, C.; Starke, U. Structural and Electronic Properties of Epitaxial Graphene on Si C (0 0 0 1): A Review of Growth, Characterization, Transfer Doping and Hydrogen Intercalation. *J. Phys. D: Appl. Phys.* **2010**, *43*, 374009–374017.
16. Kopylov, S.; Tzalenchuk, A.; Kubatkin, S.; Fal'ko, V. I. Charge Transfer between Epitaxial Graphene and Silicon Carbide. *Appl. Phys. Lett.* **2010**, *97*, No. 112109.
17. Lara-Avila, S.; Moth-Poulsen, K.; Yakimova, R.; Bjørnholm, T.; Fal'ko, V.; Tzalenchuk, A.; Kubatkin, S. Non-Volatile Photochemical Gating of an Epitaxial Graphene/Polymer Heterostructure. *Adv. Mater.* **2011**, *23*, 878–882.
18. McCann, E.; Fal'ko, V. I. Landau-Level Degeneracy and Quantum Hall Effect in a Graphite Bilayer. *Phys. Rev. Lett.* **2006**, *96*, No. 086805.
19. Guinea, F. Charge Distribution and Screening in Layered Graphene Systems. *Phys. Rev. B* **2007**, *75*, 235433.
20. Tedesco, J. L.; VanMil, B. L.; Myers-Ward, R. L.; McCrate, J. M.; Kitt, S. A.; Campbell, P. M.; Jernigan, G. G.; Culbertson, J. C.; Eddy, C. R.; Gaskill, J.; Hall, D. K. Effect Mobility of Epitaxial Graphene Grown on Silicon Carbide. *Appl. Phys. Lett.* **2009**, *95*, 122102–122103.
21. Tzalenchuk, A.; Lara-Avila, S.; Kalaboukhov, A.; Paolillo, S.; Syväjärvi, M.; Yakimova, R.; Kazakova, O.; Janssen, T. J. B. M.; Fal'ko, V.; Kubatkin, S. Towards a Quantum Resistance Standard Based on Epitaxial Graphene. *Nat. Nanotechnol.* **2010**, *5*, 186–189.
22. Zhou, S. Y.; Gweon, G. H.; Fedorov, A. V.; First, P. N.; de Heer, W. A.; Lee, D. H.; Guinea, F.; Castro Neto, A. H.; Lanzara, A. Substrate-Induced Bandgap Opening in Epitaxial Graphene. *Nat. Mater.* **2007**, *6*, 770–775.
23. Rotenberg, E.; Bostwick, A.; Ohta, T.; McChesney, J. L.; Seyller, T.; Horn, K. Origin of the Energy Bandgap in Epitaxial Graphene. *Nat. Mater.* **2008**, *7*, 258–259.
24. Zhang, Y.; Tang, T.-T.; Girit, C.; Hao, Z.; Martin, M. C.; Zettl, A.; Crommie, M. F.; Shen, Y. R.; Wang, F. Direct Observation of a Widely Tunable Bandgap in Bilayer Graphene. *Nature* **2009**, *459*, 820–823.
25. Zhou, S. Y.; Siegel, D. A.; Fedorov, A. V.; Lanzara, A. Metal to Insulator Transition in Epitaxial Graphene Induced by Molecular Doping. *Phys. Rev. Lett.* **2008**, *101*, 086402–086404.
26. Balog, R.; Jorgensen, B.; Nilsson, L.; Andersen, M.; Rienks, E.; Bianchi, M.; Fanetti, M.; Laegsgaard, E.; Baraldi, A.; Lizzit, S.; *et al.* Bandgap Opening in Graphene Induced by Patterned Hydrogen Adsorption. *Nat. Mater.* **2010**, *9*, 315–319.
27. Baskin, Y.; Meyer, L. Lattice Constants of Graphite at Low Temperatures. *Phys. Rev.* **1955**, *100*, 544.
28. Das Sarma, S.; Adam, S.; Hwang, E. H.; Rossi, E. Electronic Transport in Two-Dimensional Graphene. *Rev. Mod. Phys.* **2011**, *83*, 407–470.
29. Wang, X.-F.; Chakraborty, T. Coulomb Screening and Collective Excitations in a Graphene Bilayer. *Phys. Rev. B* **2007**, *75*, No. 041404.
30. Zerweck, U.; Loppacher, C.; Otto, T.; Grafström, S.; Eng, L. M. Accuracy and Resolution Limits of Kelvin Probe Force Microscopy. *Phys. Rev. B* **2005**, *71*, 125424.
31. Glatzel, T.; Sadewasser, S.; Lux-Steiner, M. C. Amplitude or Frequency Modulation-Detection in Kelvin Probe Force Microscopy. *Appl. Surf. Sci.* **2003**, *210*, 84–89.
32. Koehler, F. M.; Jacobsen, A.; Ensslin, K.; Stampfer, C.; Stark, W. J. Selective Chemical Modification of Graphene Surfaces: Distinction between Single- and Bilayer Graphene. *Small* **2010**, *6*, 1125–1130.
33. Burnett, T.; Patten, J.; Kazakova, O. Water Desorption and Re-Adsorption on Epitaxial Graphene Studied by SPM. 2012 arXiv:1204.3323. arXiv.org e-Print archive. http://arxiv.org/abs/1204.3323 (accessed May 2013).